



Crystal structure of the human PRPK-TPRKB complex

Jian Li ^{1,5}, Xinli Ma^{1,5}, Surajit Banerjee², Hanyong Chen¹, Weiya Ma¹, Ann M. Bode¹ & Zigang Dong ^{3,4}✉

Mutations of the p53-related protein kinase (PRPK) and TP53RK-binding protein (TPRKB) cause Galloway-Mowat syndrome (GAMOS) and are found in various human cancers. We have previously shown that small compounds targeting PRPK showed anti-cancer activity against colon and skin cancer. Here we present the 2.53 Å crystal structure of the human PRPK-TPRKB-AMPPNP (adenylyl-imidodiphosphate) complex. The structure reveals details in PRPK-AMPPNP coordination and PRPK-TPRKB interaction. PRPK appears in an active conformation, albeit lacking the conventional kinase activation loop. We constructed a structural model of the human EKC/KEOPS complex, composed of PRPK, TPRKB, OSGEP, LAGE3, and GON7. Disease mutations in PRPK and TPRKB are mapped into the structure, and we show that one mutation, PRPK K238Nfs*2, lost the binding to OSGEP. Our structure also makes the virtual screening possible and paves the way for more rational drug design.

¹The Hormel Institute, University of Minnesota, Austin, MN 55912, USA. ²Northeastern Collaborative Access Team, Argonne National Laboratory, Argonne, IL 60439, USA. ³College of Medicine, Zhengzhou University, Zhengzhou, China. ⁴China-US (Henan) Hormel Cancer Institute, Zhengzhou, China. ⁵These authors contributed equally: Jian Li, Xinli Ma. ✉email: dongzg@zzu.edu.cn

The p53-related protein kinase (PRPK, TP53RK) was initially cloned and described as a p53 interacting protein being able to phosphorylate p53 at Ser15¹. Its binding partner, Cgi121 (TPRKB, TP53RK-binding protein), was identified by the same group through a yeast two-hybrid screen². Beyond these studies, little is known about PRPK. Yet, another line of studies regarding Bud32, the yeast homologue of human PRPK, evolved rapidly. A complex referred to as EKC/KEOPS (stands for endopeptidase-like kinase chromatin-associated/kinase, endopeptidase, and other proteins of small size) was identified as a telomere regulator³ and a transcription complex⁴. This complex is composed of Bud32 (piD261, YGR262C), Cgi121 (YML036W), Kae1 (Ykr038c), Gon7 (Yjl184w), and Pcc1 (YKR095W). The EKC/KEOPS complex was later found to be essential for a universal tRNA modification, threonyl-carbamoyl adenosine (t6A), found in all tRNAs that pair with ANN codons. This modification strengthens the A–U codon–anticodon interaction on the ribosome⁵. Kae1, being an extremely well-conserved protein (TsaD/YgjD as the *E. coli* ortholog), is the catalytic subunit and transfers the L-threonyl-carbamoyl moiety to tRNA. Kae1, Bud32, and Pcc1 may be the minimum set required for t6A modification, while the addition of Cgi121 confers maximal activity. In the KEOPS complex, Kae1 switches the kinase activity of Bud32 to ATPase activity. Bud32 is responsible for the ATPase activity of the KEOPS complex and ATPase activity is required for t6A synthesis. Within the complex, Kae1 and Pcc1 form the tRNA binding core⁶.

The human version of the KEOPS complex was finalized with the identification of C14ORF142 as the Gon7 ortholog in human. Thus, the human KEOPS complex is composed of OSGEP (Kae1 in yeast), PRPK (Bud32 in yeast), TPRKB (Cgi121 in yeast), LAGE3 (Pcc1 in yeast), and GON7⁷. Surprisingly, human KEOPS complex mutations lead to Galloway–Mowat syndrome (GAMOS), a rare autosomal recessive disease characterized by early onset nephrotic syndrome and microcephaly^{8–10}. Knock-down of OSGEP, PRPK, or TPRKB inhibits cell proliferation, impairs protein translation, activates DNA damage response signaling, and reduces cell migration of human podocytes⁹.

PRPK was first shown to be phosphorylated at Ser250 and thus activated by protein kinase B (PKB/Akt)¹¹. We further demonstrated that T-LAK cell-originated protein kinase (TOPK, PBK) phosphorylates PRPK at Ser250¹². Metastatic human colon

adenocarcinomas and human cutaneous squamous cell carcinoma samples all display higher levels of Ser250 phosphorylated PRPK compared with earlier stages of colon adenocarcinomas and normal skin, respectively. Both the PRPK protein and Ser250 phosphorylation are critical for colon cancer metastasis and skin carcinogenesis in mouse models. Importantly, small molecules targeting PRPK showed promising efficacy in both models^{12–14}. Despite a central role in the synthesis of an essential tRNA modification, the elevated PRPK protein level, S250 phosphorylation level, and activity level in metastatic cancer compared to normal tissues could be preferentially targeted and toxicity to healthy cells may be minimized. In our studies, mice have benefited from the treatment using PRPK inhibitors^{13,14}. Similar to our discovery, PRPK is also highly expressed and shown as a valuable target in multiple myeloma¹⁵.

As a very promising drug target, its structure will certainly facilitate virtual screening and more rational drug development. In this study, we report the 2.53 Å crystal structure of the human PRPK–TPRKB–AMPPNP complex.

Results

Overall structure of the human PRPK–TPRKB–AMPPNP ternary complex. The human kinase superfamily (Kinome) has been grouped into eukaryotic protein kinases (ePKs) and, due to lack of sequence similarity, atypical protein kinases (aPKs)¹⁶. PRPK belongs to the ePK group labeled as “Other”. This group has certain conserved elements in their kinase domain but cannot be assigned into the major ePK groups¹⁷. Within this group, PRPK is placed in the Bud32 family, which is an ancient family with one member found in almost all eukaryotic and archaeal genomes.

Here we describe the crystal structure of human PRPK–TPRKB bound to AMPPNP (adenylyl-imidodiphosphate) at a resolution of 2.53 Å. PRPK roughly adopts a kinase domain that splits into the N-lobe and the C-lobe. The ATP analogue, AMPPNP, is bound in the cleft between the N- and C-lobe. The C-lobe is considerably smaller than a typical kinase (Fig. 1; Supplementary Fig. S1a). The TPRKB protein is comprised of a central four-stranded antiparallel β -sheet flanked by two and seven α -helices on either side (Fig. 1; Supplementary Fig. S2). TPRKB uses helices α 2, α 8, and α 9 from one side of the β -sheet

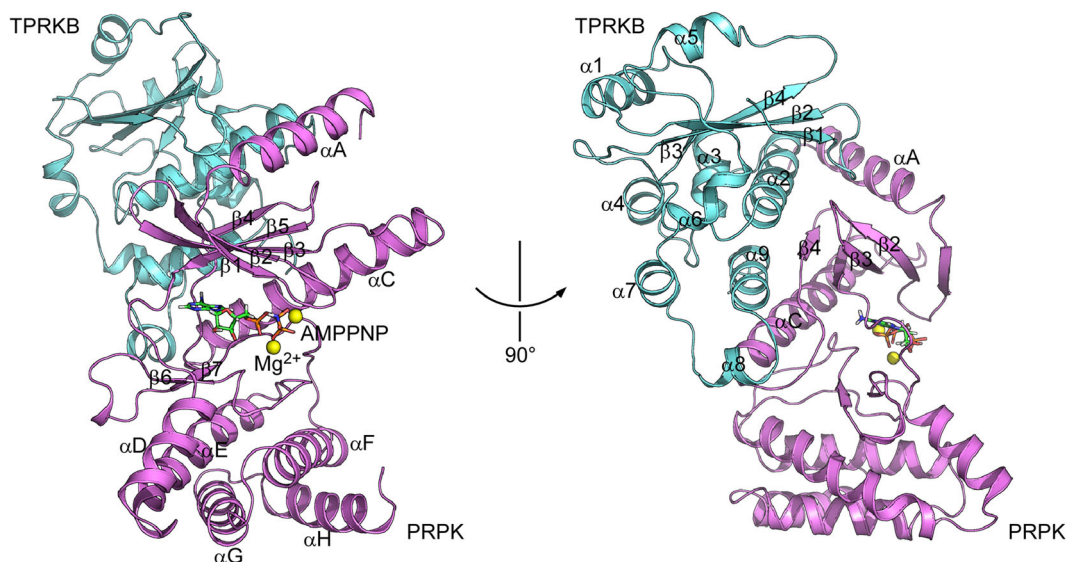


Fig. 1 Overall structure of the human PRPK–TPRKB–AMPPNP complex. PRPK adopts a kinase fold with a briefed C-lobe. TPRKB uses the β 1– β 2 loop, α 2, α 8, and α 9 to interact with the PRPK N-lobe. PRPK is colored in violet and TPRKB in aquamarine. AMPPNP is shown as stick and Mg^{2+} as yellow spheres.

and the loop between β 1– β 2 to interact with the N-lobe of PRPK (Fig. 1). The overall structure is similar to the archaeal and yeast Bud31–Cgi121 structures^{18,19}, but with unique features described below.

Conserved elements in the PRPK kinase domain. Analogous to the prototype protein kinase A (PKA), human PRPK has several conserved features. Between the β -strands β 1 and β 2 lie a conserved glycine-rich ATP-binding loop (also known as G-loop or P-loop) with the typical motif GxGxxG. The first glycine is present in ~95% of all kinases, the second in more than 99% of kinases, and the third is conserved in ~85% of kinases. The third glycine is substituted preferentially with small amino acids such as alanine or serine^{20,21}. The G-loop in PRPK is composed of 40KQGAEA⁴⁵ (Fig. 2a; Supplementary Fig. S1a). We infer that PRPK G42 corresponds to the most conserved second glycine of the consensus motif. G42 -NH forms a hydrogen bond with the A45 carbonyl oxygen, similar to the hydrogen bond between the second and third glycine in the PKA G-loop. The PRPK G-loop does not fold over to directly contact the AMPPNP γ -phosphate (~5 Å), suggesting a status not yet ready for catalysis. In PRPK, the third glycine of the G-loop motif is replaced with an alanine. Strikingly, in mammalian and zebrafish PRPK, the position of the first glycine in this motif is occupied by a lysine or glutamine, two amino acids with large sidechains. In archaea *Methanocaldococcus jannaschii* (*M. jannaschii*) this position is a standard glycine and in yeast it is a serine with a small sidechain (Supplementary Fig. S1a). Mutations localized to glycine residues in this consensus motif are known to typically disrupt the G-loop conformation and/or sterically interfere with ATP binding and are poorly tolerated²⁰. Residue K40 in human PRPK protrudes downwards from the G-loop and appears like a hindrance to the ATP binding pocket (Fig. 2c). Indeed, K40A mutation slightly increased the autophosphorylation activity of the PRPK–TPRKB complex (Fig. 2d). Thus, different types of amino acids at the position of the first glycine may reflect different activities or regulatory mechanisms of PRPK from various species. Unexpectedly, substitution of the most conserved second glycine by alanine (G42A) in the PRPK–TPRKB complex greatly stimulated its autophosphorylation activity (Fig. 2d). We could only find that in the proto-oncogene B-Raf, replacement of the third glycine with alanine shows a similar stimulatory effect²².

In PKA, an invariant lysine (K72) of the strand β 3 holds the α - and β -phosphates in position. A nearly invariant glutamate (E91) of helix α C forms a salt bridge with the invariant K72 of β 3, stabilizing its interaction with the α - and β -phosphates. The presence of this salt bridge is a prerequisite for the formation of active protein kinases²¹. These features are well preserved in our PRPK structure, suggesting an active conformation. Specifically, invariant lysine (K60) of β 3 makes direct contact with α -phosphate of AMPPNP (~2.6 Å), and E84 of helix α C forms a salt bridge with K60 (~2.8 Å; Fig. 2b). As expected, the K60A mutation almost abolished the autophosphorylation activity (Fig. 2d).

The C-lobe contains a conserved catalytic loop with the motif HxDxxxN, where D is the catalytic base that accepts the hydrogen removed from the hydroxyl group being phosphorylated. In PRPK, this motif is ¹⁶⁰HGDLTTSN¹⁶⁷ and D162 is the catalytic residue (Fig. 2a, b; Supplementary Fig. S1a). The last asparagine in this motif (N167) coordinates one of the Mg²⁺ ions used during catalysis (distance to Mg²⁺ ~2.4 Å), similar to PKA (Fig. 2b). Expectedly, the D162N mutant had dramatically reduced autophosphorylation activity (Fig. 2d).

Another conserved feature of the C-lobe is the DFG loop. The aspartate in this motif chelates one of the Mg²⁺ ions that bridges

the β - and γ -phosphates of ATP and positions the γ -phosphate for transfer to the substrate²¹. In PRPK, the exact ¹⁸³DFG¹⁸⁵ plays the same role, with the D183 sidechain carboxy oxygens in close proximity to both Mg²⁺ ions (within 2.8 Å; Fig. 2a, b; Supplementary Fig. S1a). Consistent with a critical role, the D183A mutation completely abolished the autophosphorylation activity (Fig. 2d).

In PKA, the DFG loop precedes the activation loop, which contains a phosphorylatable residue and its phosphorylation is usually required for enzyme activation. The activation loop ends with an APE (Ala–Pro–Glu) segment, which anchors the activation loop to the C-lobe. Between the phosphorylated residue and the APE motif lies the P+1 loop, which interacts with the residue adjacent to the phosphorylated residue of the peptide substrate. Although not all kinase require phosphorylation of an activation segment residue to become active, the presence of an activation loop is a typical kinase configuration²¹. Surprisingly, the activation loop is completely absent in PRPK, substituted by a 7 amino acid linker between the DFG loop and helix α F (Fig. 2a; Supplementary Fig. S1a). Helix α F is the last structural element that has an equivalent in PKA. Helix α F is a very hydrophobic helix buried inside PKA and the entire C-lobe is organized around this helix. In PRPK, the helix α F is exposed in one side and the C-lobe is further capped with helices α G– α H that follow helix α F (Fig. 2a; Supplementary Fig. S1a). Fewer structural elements after helix α F and the absence of the activation loop account for the smaller C-lobe in PRPK compared with PKA.

Nearly all active kinases contain this aforementioned K/E/D/D signature motif (K60, E84, D162, and D183 in PRPK) that plays important structural and catalytic roles²¹. These residues are extremely conserved at the primary sequence level (Supplementary Fig. S1a), at the structural level (Supplementary Fig. S1b), and at the functional level (Fig. 2d)¹⁸ in human, yeast, and archaeal Bud32. Serine/threonine-protein kinase Rio2 is one of the top structural homologs identified by the Dali server (PDB ID 4GYI, Z score 13.6, rmsd 3.3 Å, for 190 structurally aligned residues)²³. Rio2, as an atypical kinase, also lacks the activation loop and the last two helices of the canonical ePK C-lobe. Both PRPK and Rio2 have been shown to have in vitro autophosphorylation activity and ATPase activity^{6,18,24}. Lastly, PRPK has a unique extension, helix α A, preceding strand β 1. This helix is involved in the TPRKB interaction, and adopts a completely different orientation compared to the yeast Bud32–Cgi121 structure (Fig. 1; Supplementary Fig. S3a).

Coordination of the AMPPNP. Like a typical kinase, AMPPNP is well coordinated in the ATP binding pocket of PRPK. Between the adenine base of AMPPNP and the backbone of the kinase hinge region, two key hydrogen bonds are formed. Specifically, the 6-amino group of the adenine base forms a hydrogen bond with the carbonyl oxygen of E114 (~3.2 Å). The N-1 of the adenine ring forms a hydrogen bond with the main chain -NH group of the I116 hinge residue (~3.2 Å; Fig. 2c). The adenine base interacts with several hydrophobic residues in the ATP-binding pocket including V47, V58, and M113 from the N-lobe, and L169 and I182 from the C-lobe (Fig. 2c). Finally, the phosphate groups of AMPPNP and N167 and D183 sidechains are bridged by two Mg²⁺ ions (Fig. 2b). The ATP binding mechanisms are conserved among the human, yeast, and archaeal Bud32 (Supplementary Fig. S1a).

The catalytic spine and regulatory spine. Two hydrophobic “spines” are important for the structure of the active conformation of protein kinases. They are composed of amino acid

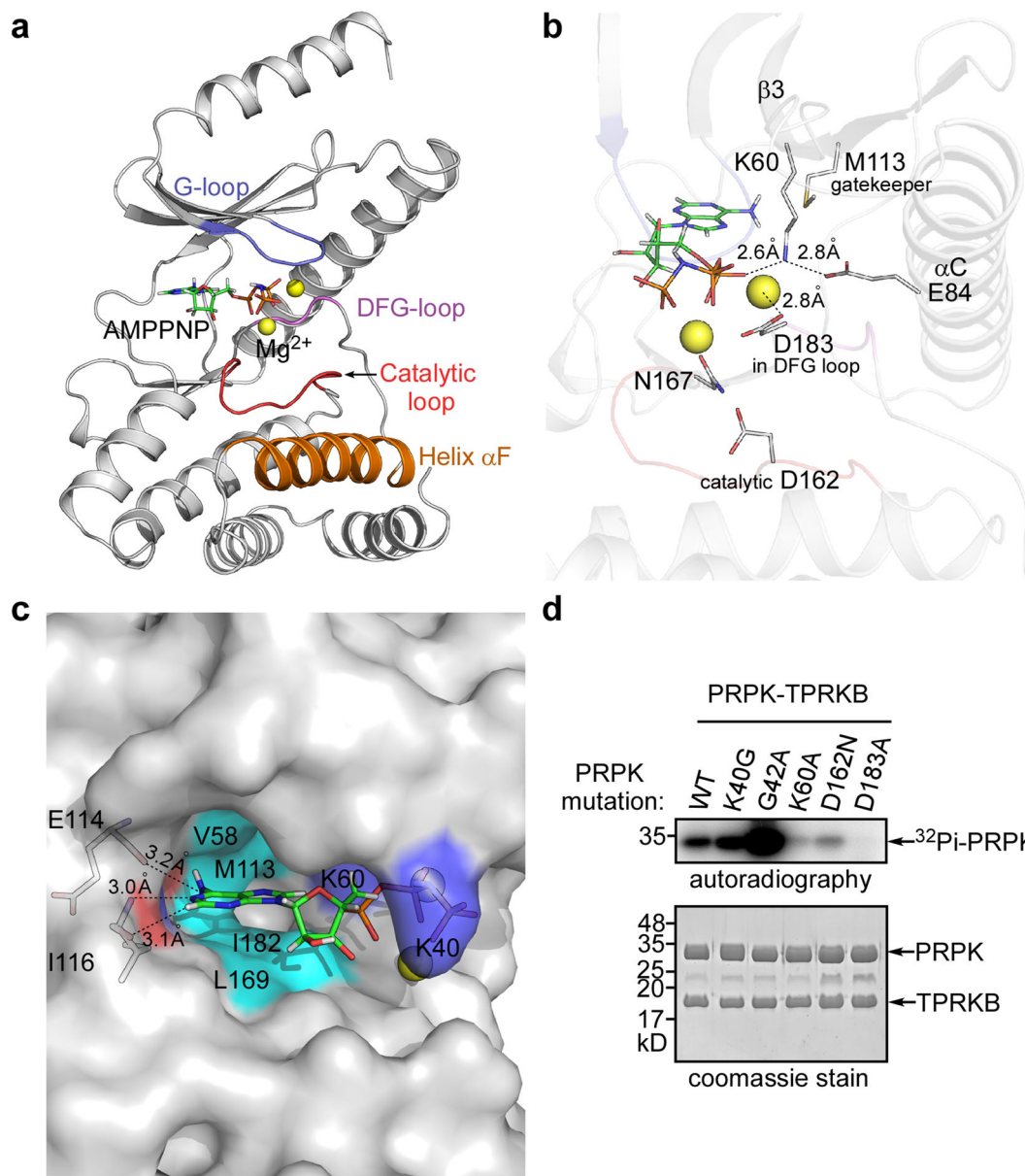


Fig. 2 The PRPK ATP binding pocket is in an active conformation. **a** Conserved kinase elements are color coded in the PRPK structure. PRPK lacks the conventional kinase activation loop between the DFG loop and helix α F. In addition, PRPK does not have the elaborated helices after α F, seen in conventional kinases. **b** Close up view of the PRPK ATP binding pocket. The invariant K60 of β 3 holds the α -phosphate of AMPPNP. K60 itself is stabilized by a salt bridge with E84 of helix α C. Two Mg^{2+} ions are coordinated by D183 of the DFG loop and N167 of the catalytic loop, respectively. D162 is the catalytic residue, and M113 is the gatekeeper residue. This configuration satisfies the requirement for an active kinase. Charged interactions are labeled with dashed lines and the distances are indicated. **c** Close up view of the PRPK ATP binding pocket in surface representation. E114 and I116 from the hinge region form hydrogen bonds with one edge of the adenine ring. The adenine base is surrounded by hydrophobic residues V47, V58, M113, L169, and I182 (V47 is on the roof of the pocket and could not be seen from this angle). Notably, the first glycine of the GxGxxG G-loop motif is replaced with K40 in human PRPK. The surface area of K40 is colored blue, and it may constitute a hindrance to ATP binding. Hydrogen bonds are labeled with dashed lines and the distances are indicated. **d** In vitro kinase assay showing the autophosphorylation activity of the wild type and mutant PRPK-TPRKB complexes. Uncropped images of gel and autoradiograph are shown in Supplementary Fig. S6.

residues that are non-contiguous in the primary structure. Both spines are assembled in the active conformation and disorganized in inactive conformations²⁵. In PRPK, the catalytic spine comprises residues V47, V58, adenine ring of AMPPNP, L169, L170, M168, V122, L203, and F207, and it is directly anchored to the carboxyl end of helix α F (Fig. 3a). The regulatory spine contains residues V101, L88, F184, and H160, and it is anchored to helix α F by a hydrogen bond between an invariant aspartate D199 in helix α F and the backbone nitrogen of H160 (~2.8 Å; Fig. 3b).

F184 of the DFG loop reaches into a pocket formed by L88 and H160, adopting a so-called DFG-in conformation, which helps maintain the D183 sidechain in a position capable of coordinating magnesium. Collectively, both spines in PRPK are well assembled, suggesting an active conformation. Indeed, the PRPK-TPRKB complex has autophosphorylation activity (Fig. 2d). However, PRPK itself only displayed extremely low autophosphorylation activity (Fig. 3c, d), and this activity could be strongly stimulated by TPRKB, similar as seen in the archaeal

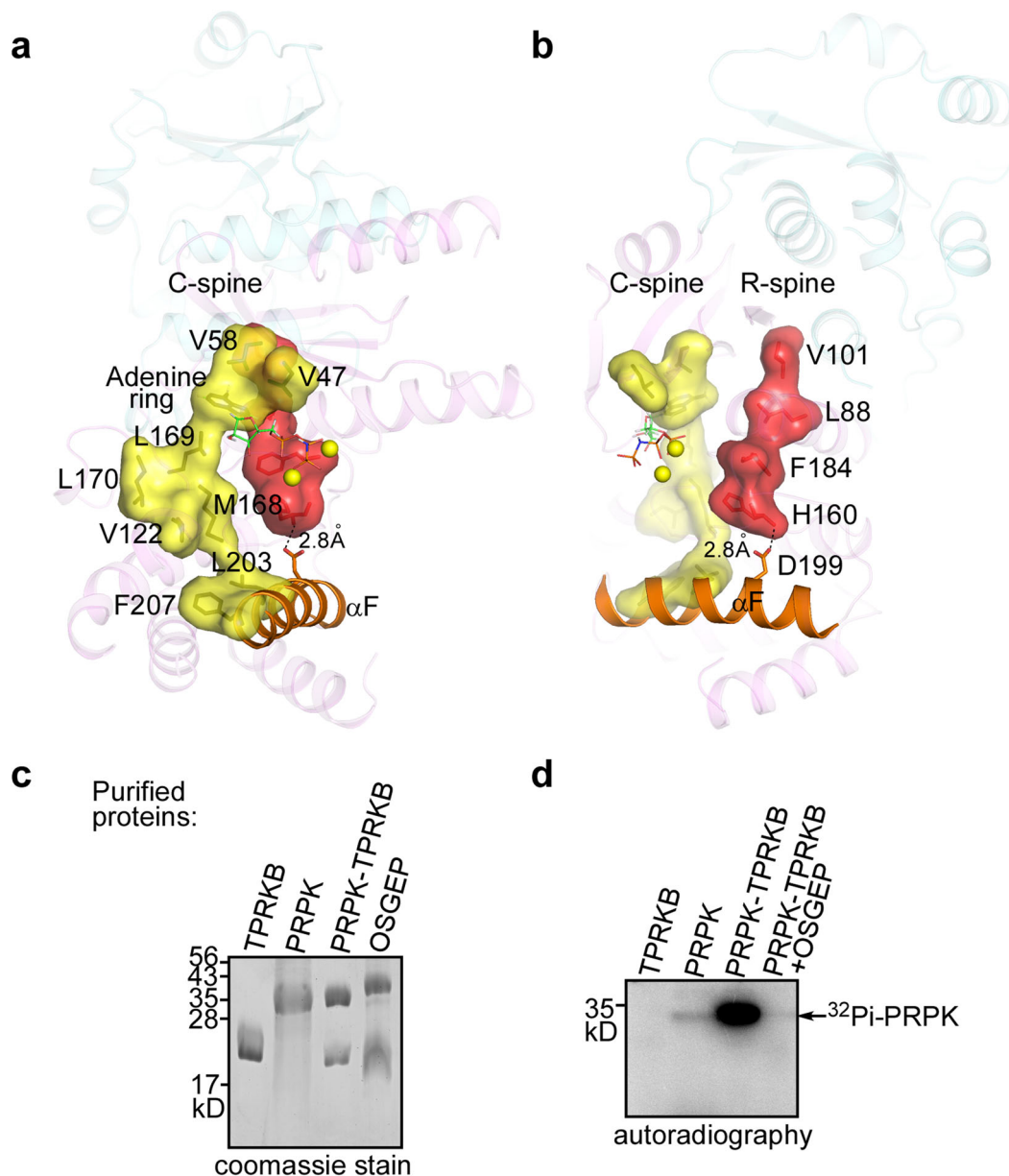


Fig. 3 Two spines of PRPK. **a** The catalytic spine (C-spine) is formed by V47, V58, adenine ring of AMPPNP, L169, L170, M168, V122, L203, and F207 (from top to bottom), and it is directly anchored to the carboxyl end of the helix α F. The C-spine is well assembled. **b** The regulatory spine (R-spine) is formed by V101, L88, F184, and H160, and it is anchored to helix α F by a hydrogen bond between the D199 carboxyl O atom and -NH group of H160 (dashed line). The R-spine is also well organized and F184 of the DFG loop adopts an active DFG-in conformation. **c** Purified proteins used in the kinase assay. **d** In vitro kinase assay showing the regulation of PRPK autophosphorylation activity by TPRKB and OSGEP. Uncropped images of gel and autoradiograph are shown in Supplementary Fig. S6.

and yeast proteins^{18,26}. Mechanistically, PRPK N-lobe makes extensive interactions with TPRKB. Particularly, PRPK residue V101 from the regulatory spine forms a hydrogen bond with TPRKB S170 (Fig. 4). Thus, TPRKB may help maintain the regulatory spine in an assembled state and the PRPK in an active conformation. One possibility is that TPRKB regulates PRPK ATP binding. Another possibility is that TPRKB does not influence PRPK ATP binding, but help position the catalytic elements ready for catalysis.

Located between the two hydrophobic spines is the gatekeeper residue deep in the ATP-binding pocket²⁵. The size of the gatekeeper residue determines the size of the binding pocket, and it is thus a gatekeeper for which nucleotides, ATP analogs, and inhibitors can bind²⁷. The gatekeeper residue in PRPK

is a methionine (M113), the same as for PKA (Fig. 2b, c; Supplementary Fig. S1a).

Interaction with TPRKB in the complex. The interface between PRPK and TPRKB, calculated by PISA, is 1423 \AA^2 ²⁸. The contact surfaces are comprised of conserved residues from both molecules (Fig. 4a, b). For PRPK, the interface is composed of β 4, a loop between β 2- β 3, and helices α A and α C, all of which are from the N-lobe (Fig. 1; Fig. 4c). For TPRKB, the interface is centered on helices α 2 and α 9 and flanked on either side by a loop between β 1- β 2 and by helix α 8 (Fig. 1; Fig. 4c). Notably, helix α 8 is a segment of loop in the TPRKB individual structure. Upon complex formation, this loop moves towards PRPK and reorganizes

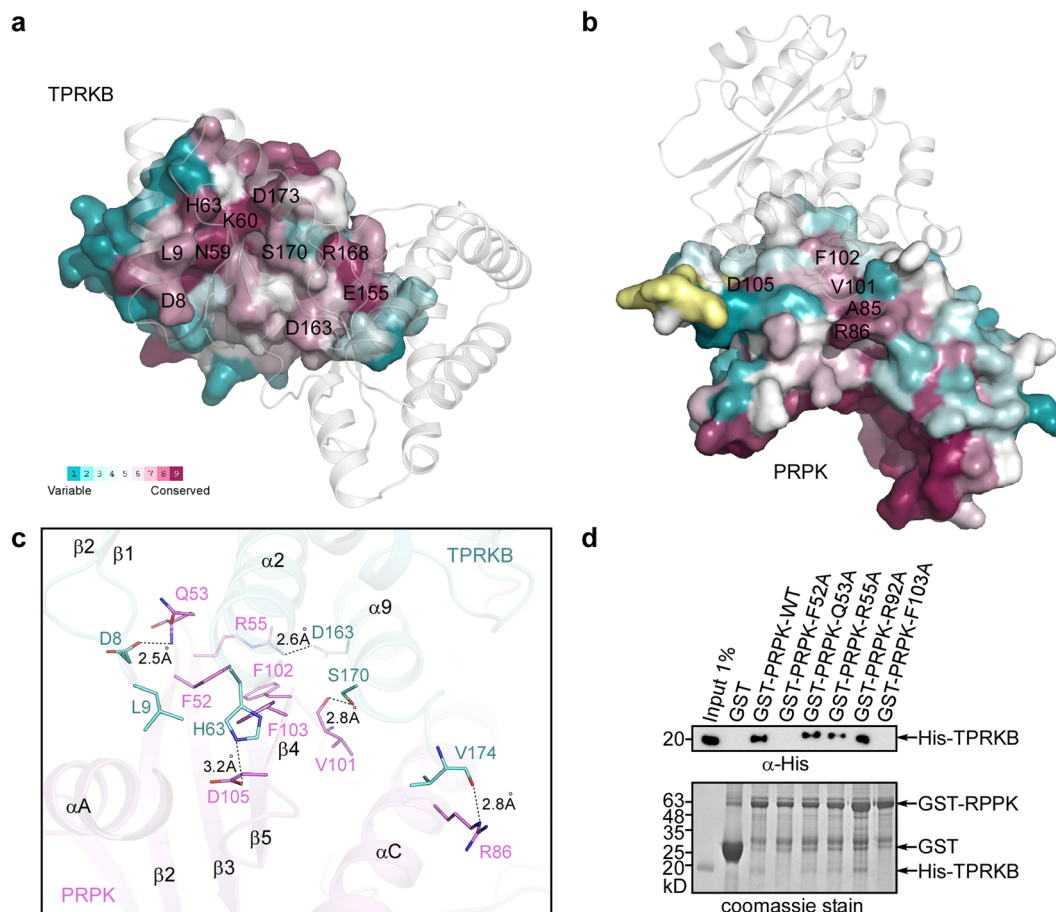


Fig. 4 Interaction between PRPK and TPRKB. **a** ConSurf style representation of the TPRKB surface involved in PRPK interaction. PRPK is shown as semi-transparent cartoon in white color. **b** ConSurf style representation of the PRPK surface involved in TPRKB interaction. TPRKB is shown as semi-transparent cartoon in white color. **c** Detailed interaction between PRPK and TPRKB. PRPK F52, F102, and F103 constitute a hydrophobic surface hosting the TPRKB helix $\alpha 2$. Hydrogen bonds are formed between PRPK Q53 and TPRKB D8, between PRPK R86 and TPRKB V174, and lastly between PRPK V101 and TPRKB S170 (dashed lines). Salt bridges link PRPK R55 with TPRKB D163, and link PRPK D105 with TPRKB H63 (dashed lines). **d** Pull-down of His-tagged TPRKB by GST-tagged PRPK mutants. GST-tagged PRPK was first immobilized on glutathione Sepharose beads and then incubated with a purified His-tagged TPRKB protein. After extensive washing, His-TPRKB bound to PRPK was detected using a His antibody. A representative result from at least three repetitions is shown. Uncropped images of gel and blot are shown in Supplementary Fig. S6.

into a helix. No other major structural change could be observed (Supplementary Fig. S3b). This is different from yeast protein, where major structural change occurs in a segment between helix $\alpha 1$ and strand $\beta 3$. This region is a short helix in the apo Cgi121 structure, but transforms into a loop in the Bud32–Cgi121 complex structure (Supplementary Fig. S3c).

In detail, a combination of hydrogen bonding, electrostatic and hydrophobic interactions contribute to the binding of two molecules. The PRPK Q53 main chain –NH forms a hydrogen bond with the TPRKB D8 side-chain oxygen atom (~ 2.5 Å). The PRPK V101 carbonyl O atom forms a hydrogen bond with the TPRKB S170 –OH group (~ 2.8 Å) and last, the PRPK R86 NE atom forms a hydrogen bond with the TPRKB V174 carbonyl O atom (~ 2.8 Å). Of the salt bridges, PRPK R55 interacts with TPRKB D163 (~ 2.6 Å) and PRPK D105 interacts with TPRKB H63 (~ 3.2 Å). Of hydrophobic interactions, PRPK F52, F102, and F103 form a hydrophobic patch on which sits the TPRKB helix $\alpha 2$. Meanwhile, TPRKB L9 at the tip of the $\beta 1$ – $\beta 2$ loop, reaches into a pocket formed by PRPK residues from helix αA and β -sheet $\beta 2$ – $\beta 5$ (Fig. 4c). The aforementioned residues account for most of the conserved amino acids seen at the contact surfaces (Fig. 4a, b). Exceptions are TPRKB N59/K60 of helix $\alpha 2$, which contact the PRPK $\beta 4$. Also, the TPRKB E155 of helix $\alpha 8$ and R168

of helix $\alpha 9$ form an intra-molecular salt bridge and contact the carboxyl end of the PRPK helix αC .

Furthermore, we selected a panel of PRPK mutations, and examined their binding to TPRKB through in vitro GST pull-down assays. Of these, mutation of two hydrophobic residues, F52A and F103A had the most dramatic effect, nearly abolishing the interaction (Fig. 4d). Collectively, we have identified two residues from PRPK, F52, and F103, that are critical for the TPRKB interaction.

Identification of methotrexate as a PRPK inhibitor through in silico screening.

With the PRPK crystal structure available, we performed virtual screening of the FDA approved drugs to identify PRPK inhibitors. Methotrexate (MTX) was identified as the second-best candidate behind ATP. Based on the GlideScore (GScore) of the docking outputs, MTX ranked higher compared with the three previously identified inhibitors^{13,14}. In the docking model, MTX fits nicely into the ATP binding pocket of PRPK. Several hydrogen bonds are formed between the MTX pteridine moiety and the PRPK hinge region, and between the MTX glutamate moiety and the PRPK G-loop (Fig. 5a, b). In vitro pull-down using Methotrexate-agarose demonstrated that MTX binds

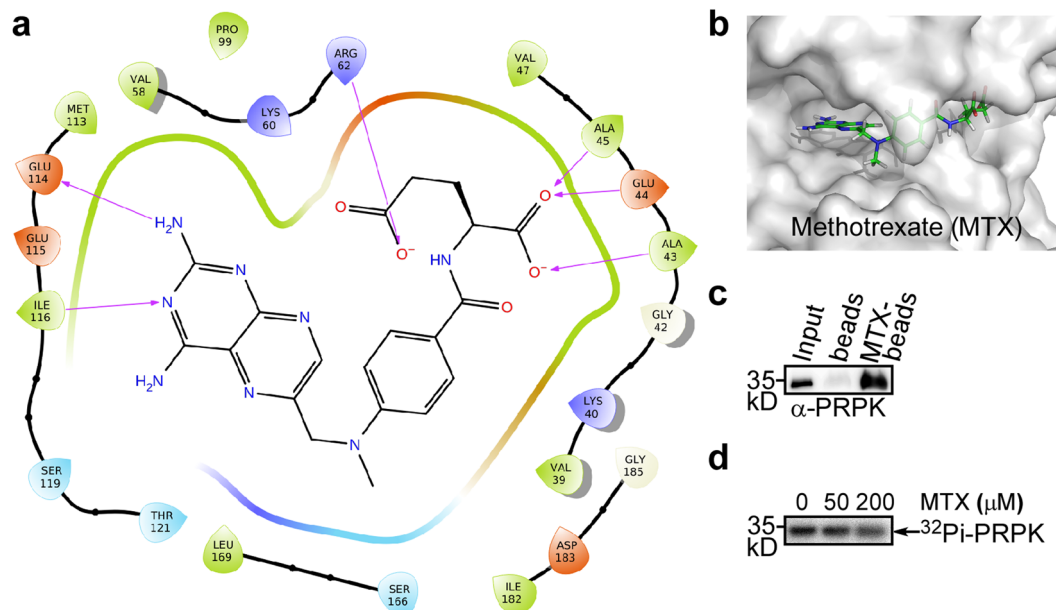


Fig. 5 Identification of methotrexate as a PRPK inhibitor. **a** Detailed MTX binding interactions with PRPK. **b** MTX fits nicely to the PRPK ATP binding pocket. **c** The binding of MTX to PRPK was confirmed by in vitro pulldown assay using MTX-agarose. **d** Inhibition of PRPK-TPRKB autophosphorylation activity by MTX. Uncropped images of blot and autoradiograph are shown in Supplementary Fig. S6.

to PRPK (Fig. 5c). MTX also showed inhibition of the PRPK-TPRKB autophosphorylation activity (Fig. 5d). Collectively, this demonstrates that virtual screening based on our PRPK-TPRKB crystal structure is very useful for lead identification.

Model of the PRPK-TPRKB-OSGEP-LAGE3-GON7 complex.

In *M. jannaschii*, PRPK and OSGEP homologues are fused into a single protein, MJ1130. The *M. jannaschii* MJ1130 Kae1 domain (mjKae1) has approximately 50% identity with human OSGEP, and the Bud32 domain (mjBud32) has 36% identity with human PRPK. By aligning our PRPK-TPRKB structure and the published OSGEP-LAGE3-GON7 structure to the 2.7 Å mjBud32-Kae1 fusion protein structure, we have built a model of the 5-protein complex (Fig. 6a). No obvious clashes are observed between PRPK and OSGEP. Notably, the PRPK surface involved in the OSGEP interaction is much more conserved than the TPRKB binding surface (Supplementary Fig. S4a; Fig. 4b). As expected, the PRPK ATP binding pocket is also highly conserved (Supplementary Fig. S4a). Upon complexation with OSGEP, the conventional substrate binding site of a kinase was completely blocked (Supplementary Fig. S4b). Indeed, upon addition of OSGEP, PRPK-TPRKB autophosphorylation activity was diminished (Fig. 3d). This is in line with the phenomenon found in yeast where Kae1 inhibits the kinase activity of Bud32²⁶ and switches the kinase activity of Bud32 to ATPase activity⁶.

The regions that PRPK uses to interact with OSGEP include the loop between β 3- α C, helix α C, the loop between β 1- β 2, a portion of the catalytic loop, helix α F, and the C-terminus of helix α H (Fig. 6b). The PRPK helix α H and the C-terminal tail are placed close to the OSGEP catalytic center and a potential regulatory mechanism will be discussed later. Through analysis of the inter-domain interactions within the mjKae1-Bud32 fusion protein structure, we focused our investigation on three pairs of salt bridges. The involved residues are conserved in human PRPK and OSGEP and are in proximity in our model. Thus, the three salt bridges may exist in the actual PRPK-OSGEP complex. For PRPK, these residues are K65, R80, and K205. To investigate this idea, we performed in vitro GST pulldown assays. As predicted,

the PRPK K65A, R80A, and K205A mutants all have reduced binding towards OSGEP (Fig. 6c). This suggests that the β 3- α C loop, helix α C, and α F are important for the OSGEP interaction and our aligned structural model is valid.

Further expanding this analysis, we included a PRPK K238Nfs*2 mutant found in several cancer cell lines and patient samples (Table 1), and also included S250A, and S250E mutants implicated in the oncogenic function of PRPK¹²⁻¹⁴. Of these, K238Nfs*2 mutation nearly abolished the interaction with OSGEP, whereas the S250A, and S250E mutations had a negligible effect (Fig. 6c).

Structure-based analysis of the disease mutations.

PRPK is frequently mutated in human Galloway-Mowat syndrome and in various cancers. We have analyzed most of these recurring mutations from a structural view and summarized our findings in Tables 1, 2. Of these, we have confirmed that the K238Nfs*2 mutation affects OSGEP binding (Fig. 6c). This mutation causes the K238 PRPK residue to change into an asparagine and residues 239 to C-terminus are deleted. Based on the homologous mjKae1-Bud32 structure and our model, the PRPK C-terminal tail directly contacts OSGEP. Previous studies in archaea and yeast systems have shown that deletion of the C-terminal tail has no impact on the PRPK-OSGEP interaction¹⁸. However, the K238Nfs*2 mutation has a longer deletion and loses half of the helix α H (Fig. 6b). In our structure, a salt bridge links K238 of helix α H and E194 of helix α F (\sim 3.0 Å) and helix α E-H forms a compact 4-helix bundle. Because the PRPK helix α F is important for the OSGEP interaction, we propose that, by disrupting the salt bridge and helix bundle, the K238Nfs*2 mutation may destabilize the C-lobe helices α H, α F, and thus abolish OSGEP binding. In yeast, Bud32 is known to be required for Kae1 catalytic activity⁶. Therefore, the PRPK K238Nfs*2 mutation also could affect OSGEP enzyme activity.

Discussion

In this study, we report the crystal structure of the human PRPK-TPRKB complex bound to AMPPNP. Our structure

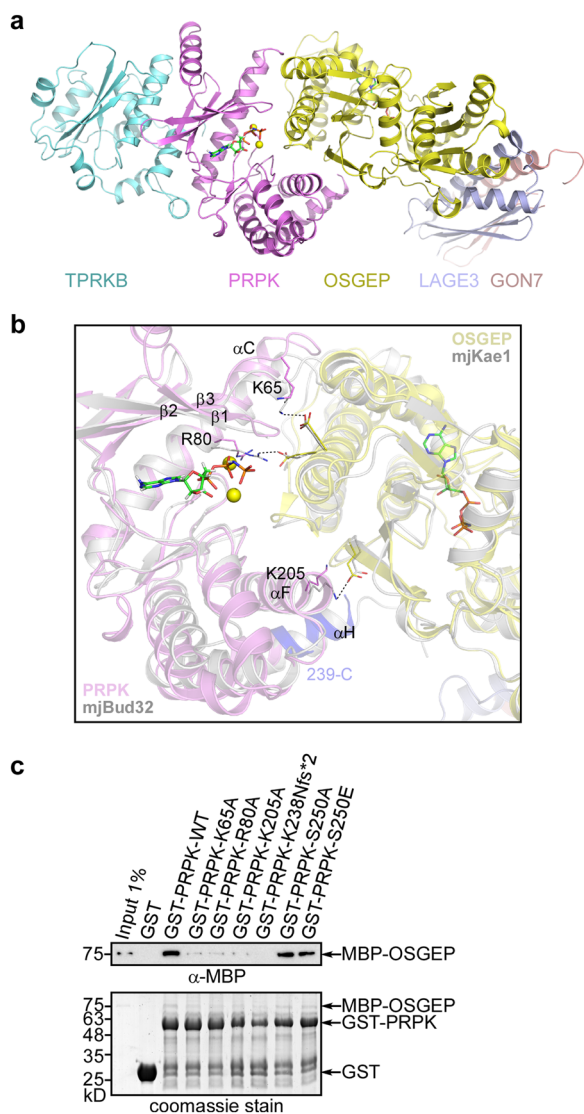


Fig. 6 A model of the human EKC/KEOPS complex. **a** The human EKC/KEOPS complex structural model, composed of TPRKB, PRPK, OSGEP, LAGE3, and GON7, is constructed by aligning our structure and the OSGEP-LAGE3-GON7 structure (PDB ID 6GWJ) to the mjBud32-Kae1 structure (PDB ID 3EN9). AMPPNP is shown as stick and Mg^{2+} as yellow spheres. **b** Detailed view of the interface between PRPK (violet) and OSGEP (yellow) in our model, aligned to the mjBud32-Kae1 crystal structure (gray). Three salt bridges found in mjBud32-Kae1 appear conserved at the PRPK-OSGEP interface. The involved residues in PRPK are K65, R80, and K205. The region deleted in the PRPK K238Nfs*2 mutant (residues 239-C) is colored light blue. **c** Pull-down of MBP-tagged OSGEP by GST-tagged PRPK mutants. GST-tagged PRPK was first immobilized on glutathione Sepharose beads and then incubated with a purified MBP-tagged OSGEP protein. After extensive washing, MBP-OSGEP bound to PRPK was detected using an MBP antibody. A representative result from at least 3 repetitions is shown. Uncropped images of gel and blot are shown in Supplementary Fig. S6.

reveals a detailed PRPK-ligand interaction and a PRPK-TPRKB inter-molecular interaction. PRPK appears in an active conformation, except that it lacks the canonical kinase activation loop. Based on our PRPK-TPRKB-OSGEP-LAGE3-GON7 model, the PRPK substrate binding site is occluded and thus may not function as a kinase in this complex. However, a PRPK-TPRKB dimer could also possibly exist in cells and could

phosphorylate substrates. In previous studies, we identified fusidic acid, rocuronium bromide, and betamethasone 17-valerate as PRPK inhibitors. These inhibitors are effective in preventing colon cancer metastasis and skin carcinogenesis^{13,14}. Here, through structure-based virtual screening, we find MTX could bind and inhibit PRPK activity. Although the specificity of MTX and its efficacy in mouse models requires further studies, this demonstrates the value of virtual screening using our PRPK-TPRKB crystal structure. MTX is widely used for chemotherapy and the treatment of rheumatoid arthritis (RA). Multiple mechanisms could be utilized by MTX²⁹. Recently, MTX has been identified as an inhibitor of the JAK/STAT pathway and may potentially be acting directly as a JAK kinase inhibitor^{30,31}. This study and ours suggest that MTX could be further exploited as a kinase inhibitor.

We previously showed that PRPK is phosphorylated by TOPK at Ser250. Wild-type PRPK, but not a PRPK S250A mutant, promotes colon cancer metastasis in a mouse model¹². In our PRPK/TPRKB structure, R245 is the last residue that could be confidently modeled. Nevertheless, in our PRPK-TPRKB-OSGEP-LAGE3-GON7 complex model, the last helix α H of PRPK is next to and oriented towards the OSGEP catalytic center (Fig. 6b; Supplementary Fig. S5b). We propose that the PRPK C-terminal tail may play a regulatory role in OSGEP activity, possibly inhibitory, and Ser250 phosphorylation may relieve the inhibition. The reason is as follows:

(a) PRPK helix α H has some conserved residues and the C-terminal tail is extremely conserved, including a nearly invariant RGR motif (PRPK residues 245–247; Supplementary Fig. S5a). Some conserved residues of helix α H could be readily explained. Both in our PRPK-OSGEP model and in the mjBud32-Kae1 crystal structure, 4 hydrophobic residues from helix α H form hydrophobic interactions with helices α F- α G. In both our model and the crystal structure, these 4 residues align well in space (Supplementary Fig. S1a; Supplementary Fig. S5a, b). This suggests that in the PRPK-OSGEP structure, PRPK helix α H and the C-terminal tail may follow a similar trajectory as the corresponding part of mjBud32 in the mjBud32-Kae1 crystal structure, including the RGR motif. In mjBud32-Kae1, the 3 amino acids are RAR, with the second arginine reaching into the Kae1 catalytic pocket. We propose that the RGR motif in PRPK also adopts a similar configuration. This is because the OSGEP/Kae1 residues surrounding the two arginines are conserved and also because the C_{α} positions of the first arginine are very closely aligned in our PRPK-OSGEP model and in the mjBud32-Kae1 crystal structure. By pointing to the OSGEP catalytic center, as in the case of the mjBud32-Kae1 crystal structure, the second arginine of the PRPK RGR motif may interfere with substrate binding and plays an inhibitory role. Continuing to follow the path of the mjBud32 tail in the crystal structure, this potentially places PRPK Ser250 close to, and PRPK M251-V252 right on top of a hydrophobic surface on OSGEP (Supplementary Fig. S5b). Phosphorylation of Ser250 may destabilize these interactions and relieve the inhibition posed by the second arginine of the RGR motif. Interestingly, serine and threonine, two phosphorylatable amino acids that frequently occupy the Ser250 position, are immediately followed by phosphomimetics glutamic acid and aspartic acid in the occurrence frequency (Supplementary Fig. S5a). Glutamic acid or aspartic acid take this position in nematodes, such as in the model organism *C. elegans*, and in several kinds of fungi. Perhaps, these species lack such a regulatory mechanism. Our hypothesis is consistent with the fact that knockdown of OSGEP and PRPK inhibits cell proliferation and reduces cell migration⁹, while phosphorylated PRPK Ser250 plays an oncogenic and S250A mutant plays an inhibitory role in metastasis^{12–14}.

Table 1 Disease mutations of human PRPK.

PRPK Mutation	Disease/tissue/functional effects	Structural effect prediction
G42D	Galloway–Mowat Syndrome ⁹	Very conserved glycine in the ATP binding G-loop of PRPK. May interfere with ATP binding and ATPase or kinase activity.
K60Sfs*61 T81R	Galloway–Mowat Syndrome ⁹ Galloway–Mowat Syndrome; failed to bind TPRKB ⁹	Large deletion. Kinase domain destroyed. Conserved residue located in helix α C. Not involved in TPRKB binding directly. May distort or destabilize α C, β 4, β 5, which are required for the binding. May also affect ATPase or kinase activity through α C.
R243L	Galloway–Mowat Syndrome ⁹	Very conserved, forms a salt bridge with E219. May affect helix α H orientation and thus OSGEP catalytic activity.
L174Wfs*4 L174Pfs*23	Truncation in 9 cases from cBioPortal curated set of non-redundant cancer studies, and 2 cell lines from cancer cell line encyclopedia (2012) ^{41,42}	Large deletion. Kinase domain destroyed.
K238Nfs*2	Truncation in 3 cases from cBioPortal curated set of non-redundant cancer studies, and 5 cell lines from cancer cell line encyclopedia (2012) ^{41,42} ; Compromised in TPRKB binding (Fig. 6c)	Part of helix α H and the conserved C-terminal tail was deleted. May affect OSGEP catalytic activity.
R152* R152P R152Q R243C	1 truncation and 4 missense mutation from cBioPortal curated set of non-redundant cancer studies ^{41,42} 2 cases from cBioPortal curated set of non-redundant cancer studies, and 1 cell line from cancer cell line encyclopedia (2012) ^{41,42}	Forms a weak hydrogen bond with G95 of α C- β 4 loop. Not very conserved. Truncation will destroy kinase domain, while mutation effect is unclear. Very conserved, forms a salt bridge with E219. May affect helix α H orientation and thus OSGEP catalytic activity.

Table 2 Disease mutations of human TPRKB.

TPRKB mutation	Disease/tissue/functional effects	Structural effect prediction
L136P	Galloway–Mowat Syndrome ⁹	Deeply buried, anchor helix α 6 to the core structure. May affect protein structural integrity.
Y149C	Galloway–Mowat Syndrome ⁹	Deeply buried, hydrophobic core formation, may affect protein structural integrity.

(b) OSGEP/Kae1 as the catalytic subunit responsible for t6A modification, is extremely conserved across all three domains of life. OSGEP has approximately 35% identity with its ortholog TsaD in *Escherichia coli* (*E. coli*), and 32% identity with *Thermotoga maritima* (*T. maritima*) TsaD. In bacteria, TsaB–TsaD–TsaE serves the same function as the eukaryotic and archaea EKC/KEOPS complex. Beyond the homologous catalytic subunit, the bacterial and eukaryotic complex both contain an ATPase subunit and, in both cases, ATP is sandwiched between the ATPase subunit and the OSGEP/TsaD subunit (Supplementary Fig. S5c). In bacteria, TsaE is a G-loop ATPase, and in eukaryotes, Bud32/PRPK could be converted from a kinase to ATPase in the complex⁶. Another similarity is that bacterial TsaB and eukaryotic Pcc1 both have the ability to dimerize. Moreover, in the bacterial TsaB–TsaD–TsaE complex, a somewhat similar regulatory mechanism exists. TsaE, the G-loop ATPase, binds at the entrance of the TsaD catalytic center, blocking access of tRNA to the site. Notably, a phenylalanine from TsaE (F64) reaches deeply into the pocket (Supplementary Fig. S5d)^{32,33}. TsaE is required for a multi-turnover t6A modification reaction, and by hydrolysis of ATP, reset TsaD to a pre-catalytic/active status^{32,34}. In our PRPK–OSGEP model, the C-terminal tail also binds and the second arginine of the RGR motif points to the OSGEP catalytic center (Supplementary Fig. 5b, d). The similarity between two t6A modification systems implies that the PRPK C-terminal tail may also block substrate binding and play an inhibitory role. These discussions are hypothetical and future studies are needed to fully address this hypothesis.

Mutations of PRPK and TPRKB are found in human Galloway–Mowat syndrome and in various cancers. We have shown that small molecules targeting PRPK showed promising efficacy in a colon cancer metastasis model and in skin cancer prevention and therapy models^{13,14}. Having a human

PRPK–TPRKB crystal structure in its liganded form will facilitate more rational drug design in the future.

Methods

Protein expression and purification. The human *RPPK* gene was a gift from Lorenzo A. Pinna³⁵. The human *TPRKB* gene was cloned from DLD-1 cells by using standard reverse transcription and PCR technologies. The human *OSGEP* gene was purchased from DNAsu (Tempe, AZ, USA). For expression, all GST-tagged constructs were cloned into the pGEX-6p-1 vector (GE Healthcare; Chicago, IL, USA) and all His-tagged constructs were cloned into the pRSFDuet-1 (Novagen; Madison, WI, USA) vector. All constructs were verified by sequencing (Integrated DNA Technologies, IDT; Coralville, IA, USA).

For structural studies, PRPK and TPRKB were ligated into the multiple cloning site I (MCSI) and MCSII of the pRSFDuet-1 vector, respectively. Thus, PRPK bears an N-terminal His tag, and the PRPK–TPRKB complex was co-expressed in the *E. coli* strain BL21–CodonPlus (DE3). Cells were cultured in Luria–Bertani (LB) medium with 50 μ g/ml kanamycin at 37 °C until the OD₆₀₀ of the culture reached 0.8–1.0. Protein expression was induced by 0.25 mM isopropyl- β -D-thiogalactopyranoside (IPTG, GoldBio; St. Louis, MO, USA) for 20 h at 16 °C. The cells were harvested by centrifugation at 4,000 rpm (Thermo Lynx 6000; Waltham, MA, USA). The pellet was resuspended with lysis buffer (20 mM Tris–HCl, pH 8.0, 400 mM NaCl, and 30 mM imidazole) and disrupted by sonication. The lysate was centrifuged at 16,000 rpm for 30 min, and the supernatant fraction was incubated with HisPur Ni–NTA resin (Thermo; Waltham, MA, USA) in batch mode for 2 h. After extensive washing with lysis buffer, the beads were collected into a 10 ml column. Target proteins were eluted with elution buffer (20 mM Tris–HCl, pH 8.0, 100 mM NaCl, and 400 mM imidazole) and then supplemented with 10 mM dithiothreitol (DTT). PRPK–TPRKB proteins were concentrated and loaded onto an anion exchange HiTrap Q HP column (GE Healthcare). Target proteins were eluted with a linear NaCl gradient and further purified using a Superdex 200 Increase 10/300 gel filtration column (GE Healthcare) in buffer containing 20 mM Tris–HCl, pH 8.0, 150 mM NaCl, and 10 mM DTT. Other His-tagged proteins were purified similarly and depending on the applications, only affinity purification and anion exchange chromatography may have been used.

GST-tagged proteins were expressed in the same fashion as PRPK–TPRKB, except that 100 μ g/ml ampicillin was used in the LB medium. The harvested cell pellet was resuspended in lysis buffer (20 mM Tris–HCl, pH 8.0, 200 mM NaCl, and 10 mM dithiothreitol (DTT)) and disrupted by sonication. The lysates were cleared by centrifugation at 16,000 rpm for 30 min and applied to glutathione Sepharose 4B

Table 3 Data collection and refinement statistics (molecular replacement).

	PRPK-TPRKB
<i>Data collection</i>	
Space group	P21
Cell dimensions	
<i>a</i> , <i>b</i> , <i>c</i> (Å)	66.86, 77.54, 100.41
α , β , γ (°)	90, 106.81, 90
Resolution (Å)	49.36–2.53(2.64–2.53) ^a
<i>R</i> _{merge}	10.7(101.7)
<i>I</i> / σ	11.1(2.0)
Completeness (%)	99.1(99.2)
Redundancy	5.1(5.1)
<i>Refinement</i>	
Resolution (Å)	2.53
No. reflections	32629
<i>R</i> _{work} / <i>R</i> _{free}	0.2114/0.2583
No. atoms	
Protein	6401
Ligand/ion	90
Water	65
<i>B</i> -factors	57.05
Protein	57.02
Ligand/ion	67.87
Water	51.41
R.m.s. deviations	
Bond lengths (Å)	0.007
Bond angles (°)	0.922

^a Values in parentheses are for highest-resolution shell

resin (GE healthcare). After extensive washing with lysis buffer, the beads were collected into a 10 ml column. On-column cleavage of the GST tag was performed by the addition of homemade PreScission protease and gentle rotation at 4°C overnight. The cleavage buffer consisted of 20 mM Tris-HCl, pH 8.0, 100 mM NaCl, and 10 mM DTT. The target proteins were eluted using the cleavage buffer and concentrated. Anion exchange chromatography (HiTrap Q HP column, GE Healthcare) and gel filtration (Superdex 200 Increase 10/300, GE Healthcare) were used sequentially to further purify the target proteins. Depending on the applications, only affinity purification may have been used and the GST tag may not have been removed.

To purify MBP-tagged OSGEP, the human *OSGEP* gene was cloned into a modified pMal-c2X vector (New England Biolabs; Ipswich, MA, USA). MBP-OSGEP was expressed in the *E. coli* strain BL21-CodonPlus (DE3). When OD₆₀₀ of the cell culture reached 0.8–1.0, protein expression was induced by 0.25 mM IPTG for 20 h at 16°C. The pellet was resuspended with lysis buffer (20 mM Tris-HCl, pH 8.0, 200 mM NaCl, and 10 mM dithiothreitol (DTT)) and disrupted by sonication. The lysates were cleared by centrifugation at 16,000 rpm for 30 min and applied to Amylose resin (New England Biolabs). After extensive washing with lysis buffer, the target proteins were eluted with 20 mM Tris-HCl, pH 8.0, 100 mM NaCl, and 10 mM maltose. Anion exchange chromatography (HiTrap Q HP column, GE Healthcare) was used to separate MBP-OSGEP from the fall-off MBP-tag. Purified proteins were flash-frozen in liquid nitrogen and stored at -80°C.

Protein crystallization and structure determination. The purified PRPK-TPRKB protein complex was concentrated to 10 mg/ml, supplemented with 1 mM AMPPNP and 2 mM MgCl₂ (final concentration), and subjected to crystallization screens by the sitting-drop vapor diffusion method at 16°C. To set up trials for crystallization, the protein was mixed with precipitant at a ratio of 1:1 using the Phoenix protein crystallography robot (Art Robbins Instruments; Sunnyvale, CA, USA). Multiple commercial kits were screened, including those from Hampton Research (Aliso Viejo, CA, USA), Jena Bioscience (Jena, Germany), and NeXtal Tubes Protein Complex Suite (Hilden, Germany). Crystals were grown in the reservoir condition of 0.1 M KCl, 0.1 M HEPES pH 7.5, 15% PEG 6000. Crystals were transferred to cryo solutions containing 25% glycerol before being flash-frozen in liquid nitrogen. X-ray diffraction data were collected at The Northeastern Collaborative Access Team (NE-CAT) beamline 24-ID-C at the wavelength of 0.979 Å. Data were processed with the NE-CAT RAPD server, which mainly uses XDS³⁶. The human PRPK-TPRKB structure was solved by the molecular replacement method using the program Phaser^{37,38}. The human TPRKB structure (PDB ID 3ENP) and *M. jannaschii* Bud32 domain structure (PDB ID 3EN9) were used as search models. Manual model building was performed using

Coot³⁹ to improve the PRPK structure. The structure was refined with Phenix refine⁴⁰, and the final 2.53 Å PRPK-TPRKB structure has a *R*_{work} and *R*_{free} of 0.211 and 0.258, respectively. Data scaling, refinement, and validation statistics are listed in Table 3.

In vitro pulldown. To examine the interactions between various PRPK mutants with TPRKB or OSGEP, GST-tagged PRPK proteins were first captured onto 20 µl glutathione Sepharose 4B resin from an appropriate amount of BL21 lysates. Then, beads with bound GST-PRPK proteins were incubated with approximately 15 µg purified His-TPRKB or MBP-OSGEP proteins in binding buffer (20 mM Tris-HCl, pH 8.0, 300 mM NaCl, 0.1% Nonidet P-40, 5% glycerol, 2 mM DTT, and 0.4 mM phenylmethanesulfonyl fluoride (PMSF)) for 2 h at 4°C. Beads were washed with binding buffer 4 times, and the bound proteins were detected by Western blotting by using anti-His (Santa Cruz, sc-8036; Santa Cruz, CA, USA) or anti-MBP (Cell Signaling #2396; Danvers, MA, USA).

To test the binding between MTX and PRPK, Methotrexate-agarose suspension from Sigma (Catalogue number M0269) was used. Glutathione-agarose resin was used as control beads. Purified PRPK-TPRKB protein (10 µg) was incubated with 20 µl compound-beads (or control beads) in binding buffer (20 mM Tris-HCl, pH 8.0, 300 mM NaCl, 0.1% Nonidet P-40, 5% glycerol, 2 mM DTT, and 0.4 mM PMSF) for 2 h at 4°C. Beads were washed with binding buffer 4 times, and the bound proteins were detected by Western blotting by using anti-PRPK (Santa Cruz, sc-514703).

In vitro kinase assay. For in vitro kinase assay, purified proteins were incubated with 5 µCi [γ -³²P] ATP (PerkinElmer, BLU002A500UC; Waltham, MA, USA) in kinase buffer containing 25 mM HEPES pH 7.4, 2 mM DTT, 0.1 mM Na₂VO₄, and 10 mM MgCl₂ for 1 h at 30°C. Reaction products were separated on SDS-PAGE gel. Gels were dried and exposed to a storage phosphor screen. The protein band with incorporated radioactivity was visualized using a Storm 840 phosphor-imager.

Computational docking. Small molecules were docked to the PRPK-TPRKB crystal structure using the docking program Glide 5.9 (Schrödinger LLC; New York, NY, USA). For docking analysis, the ATP binding site based receptor grid was generated, and ligands were prepared by the LigPrep program with default parameters (Schrödinger). Hydrogen atoms were added consistent with a pH of 7.0. Docking was achieved with default parameters in the extra precision (XP) mode¹⁴. The reported XP GScore of the ATP and MTX is -13.665 and -11.895, respectively.

Statistics and reproducibility. Proteins were purified under the same condition and all experiments were conducted in replicates as indicated. The X-ray data collection and refinement statistics were summarized in Table 3.

Reporting summary. Further information on research design is available in the Nature Research Reporting Summary linked to this article.

Data availability

The coordinates and structure factors for the human PRPK-TPRKB-AMPPNP complex were deposited in the Protein Data Bank under accession number: 6WQX. All relevant data are available from the authors upon request.

Received: 21 May 2020; Accepted: 8 January 2021;

Published online: 05 February 2021

References

1. Abe, Y. et al. Cloning and characterization of a p53-related protein kinase expressed in interleukin-2-activated cytotoxic T-cells, epithelial tumor cell lines, and the testes. *J. Biol. Chem.* **276**, 44003–44011 (2001).
2. Miyoshi, A. et al. Identification of CGI-121, a novel PRPK (p53-related protein kinase)-binding protein. *Biochem. Biophys. Res. Commun.* **303**, 399–405 (2003).
3. Downey, M. et al. A genome-wide screen identifies the evolutionarily conserved KEOPS complex as a telomere regulator. *Cell* **124**, 1155–1168 (2006).
4. Kisseleva-Romanova, E. et al. Yeast homolog of a cancer-testis antigen defines a new transcription complex. *EMBO J.* **25**, 3576–3585 (2006).
5. Srinivasan, M. et al. The highly conserved KEOPS/EKC complex is essential for a universal tRNA modification, t6A. *EMBO J.* **30**, 873–881 (2011).
6. Perrochia, L., Guetta, D., Hecker, A., Forterre, P. & Basta, T. Functional assignment of KEOPS/EKC complex subunits in the biosynthesis of the universal t6A tRNA modification. *Nucleic Acids Res.* **41**, 9484–9499 (2013).

7. Wan, L. C. et al. Proteomic analysis of the human KEOPS complex identifies C14ORF142 as a core subunit homologous to yeast Gon7. *Nucleic Acids Res.* **45**, 805–817 (2017).
8. Arrondel, C. et al. Defects in t(6)A tRNA modification due to GON7 and YRDC mutations lead to Galloway–Mowat syndrome. *Nat. Commun.* **10**, 3967 (2019).
9. Braun, D. A. et al. Mutations in KEOPS-complex genes cause nephrotic syndrome with primary microcephaly. *Nat. Genet.* **49**, 1529–1538 (2017).
10. Edvardson, S. et al. tRNA N6-adenosine threonylcarbamoyltransferase defect due to KAE1/TCS3 (OSGEP) mutation manifest by neurodegeneration and renal tubulopathy. *Eur. J. Hum. Genet.* **25**, 545–551 (2017).
11. Facchin, S. et al. Phosphorylation and activation of the atypical kinase p53-related protein kinase (PRPK) by Akt/PKB. *Cell. Mol. Life Sci.* **64**, 2680–2689 (2007).
12. Zykova, T. A. et al. The T-LAK cell-originated protein kinase signal pathway promotes colorectal cancer metastasis. *EBioMedicine* **18**, 73–82 (2017).
13. Zykova, T. et al. Targeting PRPK function blocks colon cancer metastasis. *Mol. Cancer Therapeutics* **17**, 1101–1113 (2018).
14. Roh, E. et al. Targeting PRPK and TOPK for skin cancer prevention and therapy. *Oncogene* **37**, 5633–5647 (2018).
15. Hideshima, T. et al. p53-related protein kinase confers poor prognosis and represents a novel therapeutic target in multiple myeloma. *Blood* **129**, 1308–1319 (2017).
16. Manning, G., Whyte, D. B., Martinez, R., Hunter, T. & Sudarsanam, S. The protein kinase complement of the human genome. *Science* **298**, 1912–1934 (2002).
17. Duong-Ly, K. C. & Peterson, J. R. The human kinome and kinase inhibition. *Curr. Protocols Pharmacol.* Chapter 2, Unit2 9, <https://doi.org/10.1002/0471141755.ph0209s60> (2013).
18. Mao, D. Y. et al. Atomic structure of the KEOPS complex: an ancient protein kinase-containing molecular machine. *Mol. Cell* **32**, 259–275 (2008).
19. Zhang, W. et al. Crystal structures of the Gon7/Pcc1 and Bud32/Cgi121 complexes provide a model for the complete yeast KEOPS complex. *Nucleic Acids Res.* **43**, 3358–3372 (2015).
20. Steinberg, S. F. Post-translational modifications at the ATP-positioning G-loop that regulate protein kinase activity. *Pharmacol. Res.* **135**, 181–187 (2018).
21. Roskoski, R. Jr. A historical overview of protein kinases and their targeted small molecule inhibitors. *Pharmacol. Res.* **100**, 1–23 (2015).
22. Ikenoue, T. et al. Different effects of point mutations within the B-Raf glycine-rich loop in colorectal tumors on mitogen-activated protein/extracellular signal-regulated kinase kinase/extracellular signal-regulated kinase and nuclear factor kappaB pathway and cellular transformation. *Cancer Res.* **64**, 3428–3435 (2004).
23. Holm, L. Benchmarking fold detection by DaliLite v.5. *Bioinformatics* **35**, 5326–5327 (2019).
24. Ferreira-Cerca, S. et al. ATPase-dependent role of the atypical kinase Rio2 on the evolving pre-40S ribosomal subunit. *Nat. Struct. Mol. Biol.* **19**, 1316–1323 (2012).
25. Taylor, S. S. & Kornev, A. P. Protein kinases: evolution of dynamic regulatory proteins. *Trends Biochem. Sci.* **36**, 65–77 (2011).
26. Hecker, A. et al. Structure of the archaeal Kae1/Bud32 fusion protein MJ1130: a model for the eukaryotic EKC/KEOPS subcomplex. *EMBO J.* **27**, 2340–2351 (2008).
27. Zhang, C. et al. A second-site suppressor strategy for chemical genetic analysis of diverse protein kinases. *Nat. Methods* **2**, 435–441 (2005).
28. Krissinel, E. & Henrick, K. Inference of macromolecular assemblies from crystalline state. *J. Mol. Biol.* **372**, 774–797 (2007).
29. Cronstein, B. A.-O. & Aune, T. A.-O. Methotrexate and its mechanisms of action in inflammatory arthritis. *Nat. Rev. Rheumatol.* **16**, 145–154 (2020).
30. Thomas, S. et al. Methotrexate Is a JAK/STAT Pathway Inhibitor. *PLoS ONE* **10**, e0130078 (2015).
31. Chinnaiya, K. et al. Low-dose methotrexate in myeloproliferative neoplasm models. *Haematologica* **102**, e336–e339 (2017).
32. Luthra, A. et al. Conformational communication mediates the reset step in t6A biosynthesis. *Nucleic Acids Res.* **47**, 6551–6567 (2019).
33. Missouri, S. et al. The structure of the TsaB/TsaD/TsaE complex reveals an unexpected mechanism for the bacterial t6A tRNA-modification. *Nucleic Acids Res.* **46**, 5850–5860 (2018).
34. Luthra, A. et al. Structure and mechanism of a bacterial t6A biosynthesis system. *Nucleic Acids Res.* **46**, 1395–1411 (2018).
35. Facchin, S. et al. Functional homology between yeast piD261/Bud32 and human PRPK: both phosphorylate p53 and PRPK partially complements piD261/Bud32 deficiency. *FEBS Lett.* **549**, 63–66 (2003).
36. Kabsch, W. Xds. *Acta Crystallogr. D: Biol. Crystallogr.* **66**, 125–132 (2010).
37. McCoy, A. J. et al. Phaser crystallographic software. *J. Appl. Crystallogr.* **40**, 658–674 (2007).
38. Liebschner, D. et al. Macromolecular structure determination using X-rays, neutrons and electrons: recent developments in Phenix. *Acta Crystallogr. D: Struct. Biol.* **75**, 861–877 (2019).
39. Emsley, P., Lohkamp, B., Scott, W. G. & Cowtan, K. Features and development of Coot. *Acta Crystallogr. D: Biol. Crystallogr.* **66**, 486–501 (2010).
40. Murshudov, G. N., Vagin, A. A. & Dodson, E. J. Refinement of macromolecular structures by the maximum-likelihood method. *Acta Crystallogr. D: Biol. Crystallogr.* **53**, 240–255 (1997).
41. Cerami, E. et al. The cBio cancer genomics portal: an open platform for exploring multidimensional cancer genomics data. *Cancer Discov.* **2**, 401–404 (2012).
42. Gao, J. et al. Integrative analysis of complex cancer genomics and clinical profiles using the cBioPortal. *Science signaling* **6**, pl1, <https://doi.org/10.1126/scisignal.2004088> (2013).

Acknowledgements

This work was supported by The Hormel Foundation and is based upon research conducted at the Northeastern Collaborative Access Team beamlines, which are funded by the National Institute of General Medical Sciences from the National Institutes of Health (P30 GM124165). The Pilatus 6M detector on 24-ID-C beam line is funded by a NIH-ORIP HEI grant (S10 RR029205). This research used resources of the Advanced Photon Source, a U.S. Department of Energy (DOE) Office of Science User Facility operated for the DOE Office of Science by Argonne National Laboratory under Contract No. DE-AC02-06CH11357. We also want to thank Todd Schuster, manager of the core facility of The Hormel Institute, University of Minnesota, for his efforts in maintaining the crystallization robot and in-house X-ray diffraction system.

Author contributions

J.L., X.M., and Z.D. designed the research project. J.L. and X.M. performed experiments and analyzed data. S.B. assisted in X-ray diffraction data collection. H.C. performed computational docking. W.M. assisted in performing experiments. J.L. wrote the paper, with input from A.B. and other authors. Z.D. supervised the study.

Competing interests

The authors declare no competing interests.


Additional information

Supplementary information The online version contains supplementary material available at <https://doi.org/10.1038/s42003-021-01683-4>.

Correspondence and requests for materials should be addressed to Z.D.

Reprints and permission information is available at <http://www.nature.com/reprints>

Publisher's note Springer Nature remains neutral with regard to jurisdictional claims in published maps and institutional affiliations.

 **Open Access** This article is licensed under a Creative Commons Attribution 4.0 International License, which permits use, sharing, adaptation, distribution and reproduction in any medium or format, as long as you give appropriate credit to the original author(s) and the source, provide a link to the Creative Commons license, and indicate if changes were made. The images or other third party material in this article are included in the article's Creative Commons license, unless indicated otherwise in a credit line to the material. If material is not included in the article's Creative Commons license and your intended use is not permitted by statutory regulation or exceeds the permitted use, you will need to obtain permission directly from the copyright holder. To view a copy of this license, visit <http://creativecommons.org/licenses/by/4.0/>.

© The Author(s) 2021